








Single-phase and binary phase nanogranular ferrites for magnetic hyperthermia application

Prabhakaran Thandapani^{1,2}  | Mangalaraja Ramalinga Viswanathan^{2,3}  |
 Marcus Vinícius-Araújo⁴ | Andris F. Bakuzis⁴  | Fanny Béron¹  |
 Arun Thirumurugan⁵  | Juliano C. Denardin⁶  | Jose A. Jiménez⁷  |
 Ali Akbari-Fakhrabadi⁵

¹Materials and Low-temperature Laboratory (LMBT), Institute of Physics 'Gleb Wataghin' (IFGW), The State University of Campinas (UNICAMP), Campinas, Brazil

²Advanced Ceramics and Nanotechnology Laboratory, Department of Materials Engineering, Faculty of Engineering, University of Concepcion, Concepcion, Chile

³Technological Development Unit (UDT), University of Concepcion, Coronel, Chile

⁴Physics Institute, Federal University of Goiás, Goiânia, Brazil

⁵Advanced Materials Laboratory, Department of Mechanical Engineering, University of Chile, Santiago, Chile

⁶Department of Physics, University of Santiago and CEDENNA, Santiago, Chile

⁷Department of Physical Metallurgy, CENIM-CSIC, Madrid, Spain

Correspondence

Prabhakaran Thandapani, Materials and Low-temperature Laboratory (LMBT), Institute of Physics 'Gleb Wataghin' (IFGW), The State University of Campinas (UNICAMP), Campinas, São Paulo, Brazil.
 Email: prabhakarant85@gmail.com
 and

Mangalaraja Ramalinga Viswanathan, Advanced Ceramics and Nanotechnology Laboratory, Department of Materials Engineering, Faculty of Engineering, University of Concepcion, Concepcion, 4070409, Chile.
 Email: mangal@udec.cl

Funding information

Fundação de Amparo à Pesquisa do Estado de São Paulo, Grant/Award Number: (2018) 19096-1; Fondo Nacional de Desarrollo Científico y Tecnológico, Grant/Award Number: 3160170; Fundação de Amparo à Pesquisa do Estado de São Paulo, Grant/Award Number: 2017/10581-1; Conselho Nacional de Desenvolvimento Científico e Tecnológico, Grant/Award Number: 310230/2017-9; Fundação de Amparo à Pesquisa do Estado de Goiás, Grant/Award Number: 201710267000511

Abstract

The study demonstrates the performance of heating efficiency in single-phase and binary phase spinel ferrite nanosystems. Ferrimagnetic cobalt ferrite (CoFe_2O_4) (CFO) and superparamagnetic copper ferrite/copper oxide ($\text{CuFe}_2\text{O}_4/\text{CuO}$) (CuF) nanosystems of different particle sizes were synthesized through a microwave-assisted coprecipitation method. The heating behavior was observed in range of both field amplitudes (8–24 kA/m at 516 kHz) and frequencies (325–973 kHz at 12 kA/m). The heating efficiency was analyzed and compared by means of particle size, magnetization, effective anisotropy constant, and Néel relaxation mechanism. Indeed, the heating rate was maximized in larger ferrite particles with low effective anisotropy constant. Moreover, though the magnetization and effective anisotropy constant of single-phase CoFe_2O_4 nanoparticles were higher, the binary phase $\text{CuFe}_2\text{O}_4/\text{CuO}$ nanosystems of similar crystallite size (28 nm) exhibited superior heating efficiency (4.21 °C/s). For a field amplitude and frequency of 24 kA/m and 516 kHz, the heating rate of CuF and CFO ferrites with different crystallite sizes decreased in the order of $4.21 > 2.14 > 0.58 > 0.52$ °C/s for $29 \text{ nm} > 25 \text{ nm} > 12 \text{ nm} > 15 \text{ nm}$, respectively. The results emphasize that binary phase ferrite nanoparticles are better thermoseeds than the single-phase ferrites for the magnetic hyperthermia application.

KEYWORDS

anisotropy, heat conduction, magnetic measurements, magnetically ordered materials, nanostructured materials, precipitation

1 | INTRODUCTION

In the current scenario, the death rate due to cancer increases every year and it is estimated that 9.6 million deaths occurred in 2018 as per the information published by World Health Organization (WHO).¹ They infer that approximately 70% of deaths due to cancer happen in low and middle-income countries owing to the treatment unavailability and screening processes.¹ Early-stage diagnosis of cancer is most likely to increase the survival with less expensive treatment, whereas the later stage diagnoses mostly fail to proceed with curative treatment. After diagnosis, a patient may undergo specific treatment techniques such as surgery, radiotherapy, chemotherapy, hyperthermia, and targeted drug delivery depending on the tumor cell type. Malignant cancer cells are locally destroyed without affecting the native healthy cells, whereas the side effects associated with these treatment processes have also been addressed.²⁻⁴ In this context, the hyperthermia is an effective method to increase the temperature of the affected zone of a human body until 39 to 45°C, which is sufficient to kill locally the tumor cells by a suitable alternating magnetic field amplitude and frequency.⁵

Magnetic hyperthermia is one of the promising methods in cancer treatment, in which magnetic nanoparticles (NPs) play a crucial role to achieve the desired goal. The demand for biocompatible and efficient magnetic NPs for clinical uses increases every year. Spinel ferrite NPs are widely being studied due to their moderate magnetic and microwave properties. They have various potential applications such as in magnetic sensors, recording media, microwave absorbers, catalysis, as well as in biomedical applications like magnetic resonance imaging, diagnosis, drug delivery, and magnetic hyperthermia treatment.^{6,7} Various magnetic NPs such as Fe_3O_4 , $\gamma\text{-Fe}_2\text{O}_3$, MnFe_2O_4 , CoFe_2O_4 , CuFe_2O_4 , NiFe_2O_4 , ZnFe_2O_4 , $\text{Zn}_x\text{Mn}_{1-x}\text{Fe}_3\text{O}_4$, and Zn-Mn-Gd-doped iron oxide NPs,⁸⁻¹⁵ as well as exchange-coupled ferrites like $\text{CoFe}_2\text{O}_4/\text{Fe}_3\text{O}_4$, $\text{MnFe}_2\text{O}_4/\text{CoFe}_2\text{O}_4$, $\text{Zn}_{0.4}\text{Co}_{0.6}\text{Fe}_2\text{O}_4/\text{Zn}_{0.4}\text{Mn}_{0.6}\text{Fe}_2\text{O}_4$, etc, are reported for magnetic hyperthermia application.¹⁶⁻²⁰ It is observed that the heating efficiency depends on the key parameters inherent to NPs, such as particle size, particle size distribution, saturation magnetization, anisotropy constant, morphology/shape, particle-particle interaction, chemical composition, exchange interaction, etc.^{8,21} Since the magnetic field amplitude and frequency are not inherent to the NPs, the maximum heating efficiency may be achieved for different values in different ferrite NP systems.²² Although various research reports are found in the literature to study this effect on heating performance, fine-tuning these parameters by developing inexpensive and novel ferrite NPs that show higher heating efficiency under small field amplitude and frequency would be useful for the research field advancement.

Among the spinel ferrites, cobalt ferrite nanoparticles attracted the researchers due to their moderate saturation

magnetization, coercivity, and magnetocrystalline anisotropy constant with better chemical and physical stability,^{11,23,24} whereas copper ferrite nanoparticles exhibit low coercivity, good biocompatibility, and better magnetic response at low field amplitudes, which make them ideal candidates for magnetic hyperthermia.^{6,8,25} The biocompatibility of copper-based nanoparticles such as CuO , Cu_2S ,²⁶⁻²⁹ and copper ferrites have been analyzed with human cell models.^{30,31} On the other side, cobalt-based ferrites need to be coated with biocompatible ligands for the clinical tests.³² The results showed that chosen ferrites exhibited less cytotoxicity. However, it varies upon the concentration of control system used for the analysis. Apart from the single-phase ferrite nanoparticle heating performance, the exchange-coupled hard/soft or soft/hard magnetic phases might contribute to enhance the heating efficiency for real-time applications.^{16,33,34}

Hence, the present work is intended to study the heating efficiency of two ferrites systems: single-phase cobalt ferrite (CoFe_2O_4) (CFO) nanoparticles and binary phase copper ferrite/copper oxide ($\text{CuFe}_2\text{O}_4/\text{CuO}$) (CuF) nanogranular systems. Two sample sets with different crystallite sizes in each composition were synthesized through a microwave-assisted co-precipitation method with a shorter reaction time of 7 minutes. The chosen method is well established to achieve ferrite nanoparticles exhibiting almost homogeneous shape and a narrow particle size distribution.^{35,36} Two different samples of CFO nanoparticles synthesized with and without urea exhibit the same magnetization. Similarly, each CuF nanogranular systems obtained from different volume of precursors also show magnetization close one to another. Nevertheless, the effects of particle size, effective anisotropy constant, and Néel relaxation behavior on heating efficiency have been addressed in this report. Heating curves were recorded varying both field amplitude and frequency to investigate the dry NP behavior toward the measurement conditions. Although the range of field and frequency is out of clinical tests, focus of the manuscript is to address mainly the potential of chosen nanoferrites for hyperthermia applications. To the best of our knowledge, no article is found in the literature that discusses the heating efficiency of binary phase $\text{CuFe}_2\text{O}_4/\text{CuO}$ nanogranular systems. Comparative studies reveal that larger crystallite size $\text{CuFe}_2\text{O}_4/\text{CuO}$ NPs exhibit superior heating efficiency than that of single-phase CFO NPs with higher effective anisotropy constant.

2 | MATERIALS AND METHODS

All the chemicals were purchased from Sigma-Aldrich and used without further purification. Cobalt nitrate hexahydrate ($\text{Co}(\text{NO}_3)_2 \cdot 6\text{H}_2\text{O}$) 98%+A.C, iron nitrate nonahydrate ($\text{Fe}(\text{NO}_3)_3 \cdot 9\text{H}_2\text{O}$) 98%, copper nitrate trihydrate ($\text{Cu}(\text{NO}_3)_2 \cdot 3\text{H}_2\text{O}$)

99%, sodium hydroxide (NaOH) pellets $\geq 98\%$ ACS grade, and urea were used as the starting materials. Millipore water was used as a solvent during the synthesis.

2.1 | Synthesis of cobalt ferrite nanoparticles

CFO nanoparticles of different sizes were prepared through a microwave-assisted co-precipitation method as reported earlier in references.^{35,36} In brief, the aqueous cobalt and iron nitrate solutions were mixed stoichiometrically and stirred for $\frac{1}{2}$ hour. Then, 2.52 mol/L of NaOH solution was added while stirring and the process was extended for $\frac{1}{2}$ hour. The obtained suspension with 60 mg of urea or without urea was transferred to an alumina crucible and subjected to microwave irradiation for 7 minutes. In this study, urea is used as capping agent as it exhibited control over the structural and magnetic properties of CFO nanoparticles as reported elsewhere.^{35,36} A domestic microwave oven model SOMELA (Mirage 1700 DM), with a power of 700 W, was used as irradiation source. The final black precipitates were allowed to cool down to room temperature, before being washed with Millipore water, filtered, and dried at 100°C for 3 hours. The samples are denoted as CFO_UR and CFO_U0 for CFO synthesized with (UR) and without (U0) 60 mg of urea, respectively.

2.2 | Synthesis of copper ferrite nanoparticles

The same microwave-assisted coprecipitation method was also used for the synthesis of copper ferrite NPs of different sizes. In this case, 0.2 mol/L of copper nitrate and 0.4 mol/L of iron nitrate solutions were prepared separately in 20 or 40 mL of aqueous medium yielding CuF_20 and CuF_40 samples, respectively. The solutions were mixed and stirred for $\frac{1}{2}$ hour before 2.52 mol/L of 20 mL aqueous sodium hydroxide solution was slowly added drop by drop while vigorous stirring at room temperature. The suspension was stirred for additional $\frac{1}{2}$ hour, then transferred to an alumina crucible and subjected to microwave irradiation for 7 minutes. The product was allowed to cool down naturally, washed multiple times, centrifuged and finally dried at either 80°C for 18 hours (CuF_20) or 100°C for 15 hours (CuF_40). Here, the different volumes of aqueous medium and drying temperatures were used to yield different sizes of CuF systems.

2.3 | Characterization

The ferrite nanoparticle characterization involved structural and morphological states, coupled with magnetic and

hyperthermia behaviors. X-ray diffraction (XRD) patterns were obtained using Cu-K α radiation for 2θ value range from 10 to 80° with a step of 0.02° using a Bruker-AXS 104025-0 diffractometer. The observed diffraction patterns were fitted by the Rietveld method to a structural model consisting of a combination of cubic spinel copper ferrite (CuFe₂O₄) and tenorite (CuO) or cubic spinel cobalt ferrite (CoFe₂O₄), using the version 4.2 of the program TOPAS (Bruker AXS) and crystallographic information obtained from Pearson's Crystal Structure Database for Inorganic Compounds.³⁷ The best fit was selected on the basis of agreement factors and stability of the refinement, using goodness of fit (GOF, whose limit tends to 1), the statistically expected least-squares fit (R_{exp}), the weighted summation of residual of the least-squares fit (R_{wp}), and the profile residual (R_p). The crystallite size was estimated by Scherrer's equation from the respective peak positions.

On the other side, the NP morphology was obtained using transmission electron microscope (TEM) (Tecnai F20 FEG TEM) with 200 kV accelerating voltage. The average particle size was estimated from different micrographs of the sample using ImageJ software. Moreover, the mole percentage of elements was obtained using wavelength-dispersive X-ray spectrometer (WDX) Model S8 TIGER, BRUKER. For the measurements, ferrite nanoparticles were dispersed in ethanol/polyvinylpyrrolidone (PVP) solution and sonicated for $\frac{1}{2}$ hour. The ferrite films were coated over the silicon substrate using a drop casting method at approximately 80°C. Two hours dried films were used for the WDX analysis.

Finally, the magnetic measurements were carried out using a Quantum Design MPMS 7T magnetometer, whereas the magnetic hyperthermia data were recorded using a Nanothermics model Magnetherm instrument. The heating curves were obtained for 25 mg of dry powder nanoparticles at different frequencies (325, 516, 729, and 973 kHz) and magnetic field amplitudes (8, 12, 16, 20, 24 kA/m). The heating rate was estimated by neglecting the initial 10 seconds of measurement and performing a linear fitting on the following next 10 seconds of data. The temperature was monitored with fluoroptic thermometer using Model Luxtron m3300.

3 | RESULTS AND CHARACTERIZATION

3.1 | Structural analysis

Both CFO nanoparticle XRD patterns present only cobalt ferrite diffraction peaks, which corresponding crystal planes are indexed (Figure 1A). Moreover, Rietveld refinement profiles convey that both samples (CFO_UR and CFO_U0) consist of single-phase cobalt ferrite nanoparticles with a fcc cubic spinel structure with similar lattice

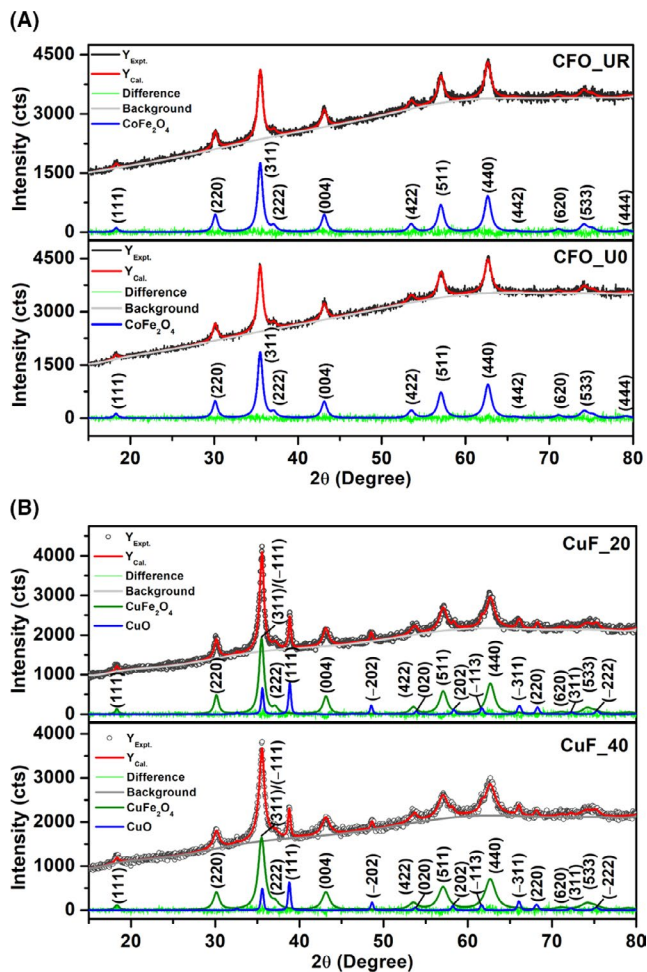


FIGURE 1 Rietveld refinement on X-ray diffraction patterns of (A) Cobalt ferrite and (B) $\text{CuFe}_2\text{O}_4/\text{CuO}$ nanogranular system

parameter but with bigger size when synthesized with urea (Table 1). This confirms that CFO NPs prepared through both procedures yield pure NPs.

On the other side, the copper ferrite nanoparticles synthesized through a microwave-assisted coprecipitation method exhibit binary phases with a few fractions of monoclinic structure tenorite phase (CuO) and higher phase of cubic spinel CuFe_2O_4 , as it is evidenced from the Rietveld refinement profile shown in Figure 1B and Table 1. Even if CuO crystallite sizes are similar in both systems (CuF_20 and CuF_40), increasing the aqueous solution quantity decreases the CuFe_2O_4 one, while keeping a closely matching lattice constant. We believe that the metal salt dissolution was better achieved with 40 mL of aqueous medium, leading to more nucleation centers for CuFe_2O_4 formation. This situation would favor yielding a smaller crystallite size. Therefore, the present experimental procedure is useful to prepare $\text{CuFe}_2\text{O}_4/\text{CuO}$ binary phase nanogranular systems as reported in the literature.^{38,39}

To further validate the sample compositions, they were subjected to WDX analysis. The results show that the concentrations of Co (29 mol %) and Fe (71 mol %) elements are similar in both CFO_U0 and CFO_UR cobalt ferrite samples. However, $\text{CuFe}_2\text{O}_4/\text{CuO}$ binary phase CuF_20 (CuF_40) ferrites have different mole percentages: 24 (34)% and 76 (66)% for Cu and Fe elements, respectively. It proves that stoichiometric CFO ferrites are achieved, whereas in the case of CuF ferrites, nonuniform composition is obtained. This result supports the data presented in Table 1.

Concerning the nanoparticle morphology, we observe from TEM micrographs that both ferrite NPs are composed of spherical and/or cubic-like morphologies with agglomerations, whereas $\text{CuFe}_2\text{O}_4/\text{CuO}$ systems are forming intricate-like structures (Figure 2). The particle size estimated using ImageJ software revealed that the present synthesis method yields CFO and CuF with a particle size distribution of 7–26 nm and 4–40 nm, respectively. Consistently with XRD analysis, the average particle size estimated from TEM

TABLE 1 Structural properties of ferrites

Sample	Composition	Crystallite size from XRD (nm)	Particle size from TEM (nm)	Lattice parameter (Å)	R_{exp}	R_{wp}	R_p	GOF	Composition (%)
CFO_UR	CoFe_2O_4	15.0	14.0 ± 1.7	8.387	1.88	1.89	1.50	1.01	100
CFO_U0	CoFe_2O_4	12.0	12.0 ± 1.1	8.380	1.84	1.88	1.49	1.02	100
CuF_20	CuFe_2O_4	29.0	19.0 ± 6.4	8.385	2.30	2.41	1.93	1.05	85
	CuO	28.0							
CuF_40	CuFe_2O_4	21.0	15.0 ± 4.7	8.389	2.30	2.39	1.90	1.04	89
	CuO	29.0							

micrographs decreases in the absence of urea or increasing aqueous solution quantity, in CFO and CuF cases, respectively (see Table 1). However, while XRD and TEM yield similar average particle size values for CFO samples, the TEM results are inferior to the XRD ones in the case of both CuF samples. It is possible that CuF samples might be composed of tiny particles surrounded by less crystalline particles. Moreover, it could be due to the different techniques involved in the crystallite size/particle size analyses. Nevertheless, the structural analyses evidence that the particle sizes of ferrite systems were successfully modified.

3.2 | Magnetic analysis

The zero-field cooled (ZFC) and field cooled (FC) magnetization curves, recorded in the temperature range of 5–320 K, depict that CFO NPs exhibit superparamagnetic behavior above 320 K (Figure 3A), whereas binary CuF nanosystems are showing a blocking temperature (T_B) and an irreversibility temperature (T_{irr}), as depicted in Figure 3B. The T_B and T_{irr} variations are typically due to different particle size distributions of CuFe_2O_4 and CuO phases in CuF NPs (see Table 1). The T_B value of the present CuF_20 is very close to the value previously reported for CuFe_2O_4 NPs of similar crystallite size.⁴⁰

Field-dependent magnetization curves of ferrite nanoparticles were acquired at 300 and 5 K (Figure 3C–F), where the loops at 5 K were measured under field cooled condition in an external magnetic field of 8 kA/m. Figure 3 and the related Table 2 evidence that cobalt ferrite NPs exhibit ferrimagnetic nature, whereas binary CuF nanogranular systems show superparamagnetic-like behavior with negligible coercive field and remanence magnetization at 300 K, though their crystallite size is larger than CFO. The blocked state of both binary CuF nanogranular systems is clearly observed at 5 K (inset of Figure 3E–F). Despite the crystallite size difference, both cobalt ferrite NPs exhibit magnetization close to each other. Similarly, both binary CuF nanogranular systems also found to exhibit similar magnetization at 300 and 5 K, where the particle size and composition-dependent magnetization of CuF systems compensate each other (see Tables 1 and 2). The magnetic contribution of CuO cannot be neglected, as it was previously evidenced based on magnetization measurements.⁴¹ In ferrite systems, smaller crystallite or particle size variation yielded moderate change in coercive field at 5 K.

It is possible that for smaller crystallite size, the effects of surface spin disorder, canting effects and anisotropy constant might be more important due to larger surface to volume ratio. Consequently, it promotes more pinning effects along the field direction, thus leading to an increased coercivity.

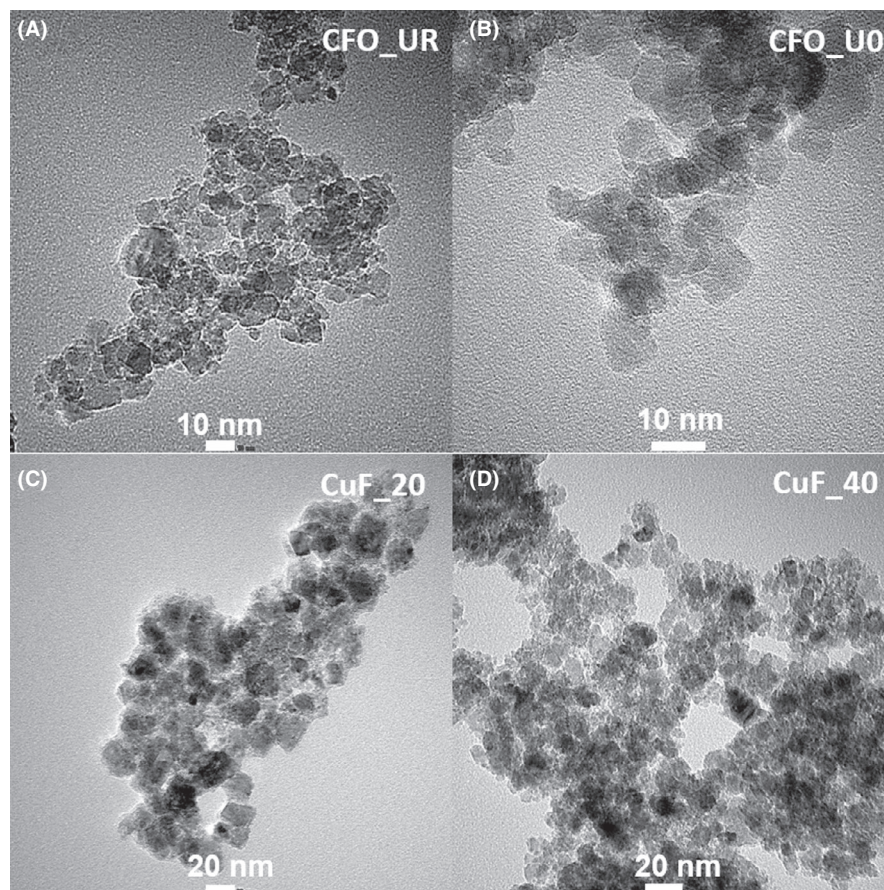


FIGURE 2 Typical nanoparticle TEM micrographs (A) CFO_UR, (B) CFO_UO, (C) CuF_20, and (D) CuF_40

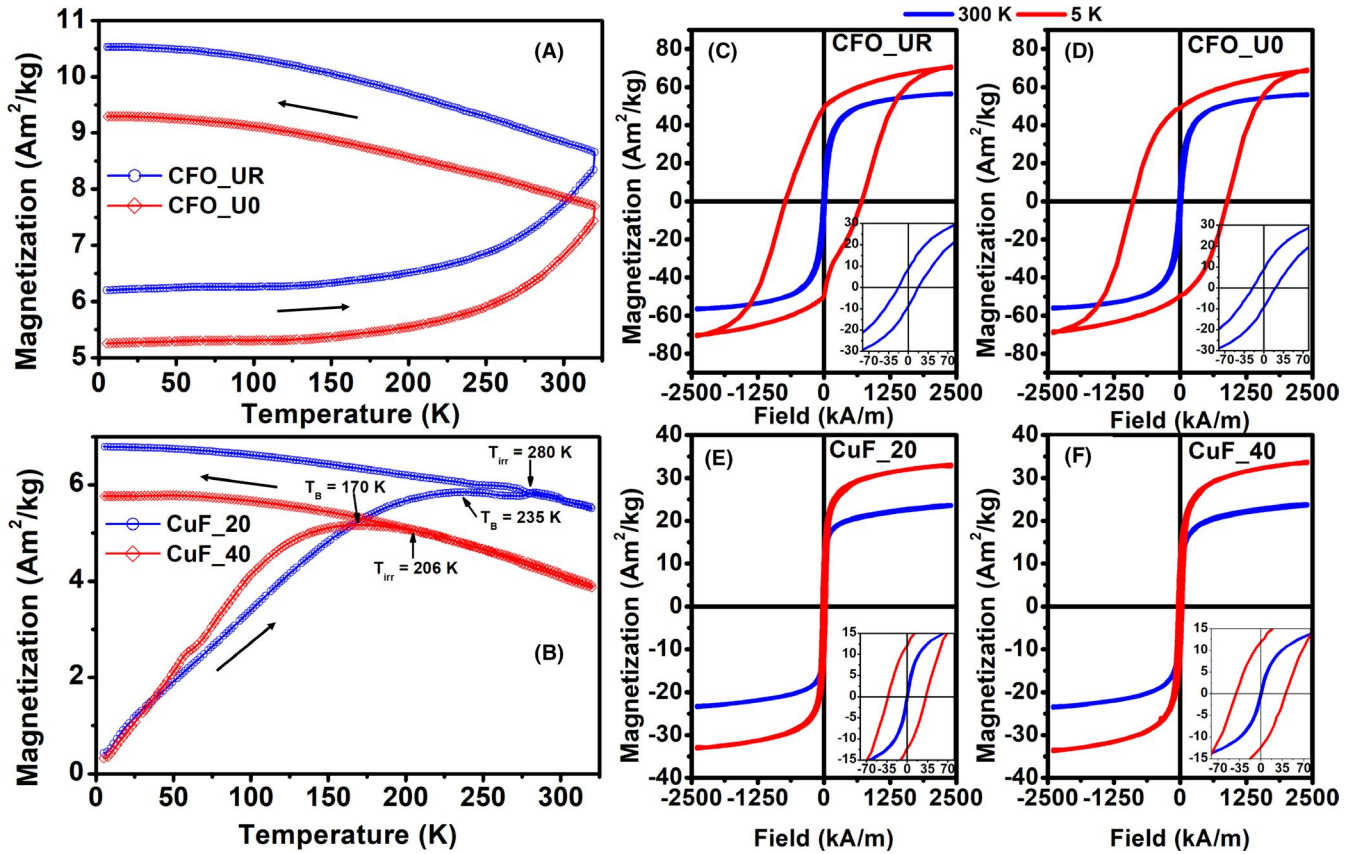


FIGURE 3 (A-B) ZFC-FC curves under 8 kA/m and (C-F) magnetic hysteresis loops of ferrite systems

Samples	Saturation magnetization (Ms) (Am ² /kg)		Coercive field (Hc) (kA/m)		Remanence magnetization (Am ² /kg)		K_{eff} (J/m ³)	$\tau_N \times 10^{-8}$ s
	300 K	5 K	300 K	5 K	300 K	5 K		
CFO_UR	56.2	70.9	17.37	711.13	8.7	49.5	3.46×10^5	1.47
CFO_U0	55.8	68.3	20.43	889.03	8.8	49.0	4.17×10^5	0.58
CuF_20	23.5	32.8	—	32.36	0.6	12.1	7.48×10^3	0.14
CuF_40	23.6	33.4	—	40.14	0.5	11.9	9.63×10^3	0.13

TABLE 2 Magnetic properties of ferrite NPs, extracted from Figure 3 hysteresis curves

The disordered surface spins may influence the surface anisotropy with particle size variation and thus the effective magnetocrystalline anisotropy constant (K_{eff}).²¹ K_{eff} at a given temperature is calculated using the saturation magnetization (M_s) and coercive field (H_c), as follows;⁴²

$$K_{\text{eff}} \cong \frac{H_c M_s}{0.96} \quad (1)$$

In the present ferrite nanoparticle systems, K_{eff} varies in accordance with the coercive field since the saturation magnetization of ferrites remains fairly constant (Table 2). The samples CFO_U0 and CuF_40 show the maximum K_{eff} values (respectively, 4.17×10^5 and 9.63×10^3 J/m³ at 5 K).

However, the estimated K_{eff} values are one order less than the values reported for cobalt and copper ferrites.⁸

To verify the magnetic transition of ferrite systems, ZFC magnetization derivatives are plotted in Figure 4. It reveals that cobalt ferrite NPs are not exhibiting any observable change in the whole-temperature range. However, binary CuF nanogranular systems show magnetic transitions due to CuO and CuFe₂O₄. First, the tenorite phase (CuO) normally undergoes transitions at 213 and 230 K, which correspond to the commensurate collinear antiferromagnetic order (AF1) and incommensurate nonlinear spiral antiferromagnetic order (AF2), respectively.^{38,43-45} In the case of CuF_20 (CuF_40), the onset temperature of AF1 to AF2 transition begins at 255 (225) K with the maximum transition at 275 (290) K, whereas

another transition which corresponds to AF2 to paramagnetic order state is found at 305 (310) K. Similar to our results, paramagnetic to AF1 state of CuO has been observed at 250 K under zero-field condition.⁴⁶ The transition is more distinct in the CuF_20 system, which presents similar particle sizes of CuFe₂O₄ and CuO and a higher percentage of tenorite phase (15%). Moreover, it is also important to mention that while the maximum transition in CuF_20 is observed close to T_{irr} , it is far higher in the CuF_40 case. Therefore, it suggests that the observed transitions are owing to the CuO phase.

Second, the anomalous downward magnetization observed at 60 K (CuF_40) is attributed to the freezing temperature (T_F) of more surface spin disordered in CuFe₂O₄ NPs.⁴⁰ Since this phenomenon occurs at higher temperature for larger crystallite size (105 K for CuF_20), it supports the possible reason for higher coercivity in CuF_40 compared to CuF_20 binary system. Moreover, the magnified views of field-dependence magnetization curve (Figure 3E-F) depict that the strong exchange-coupled interaction between CuFe₂O₄ and CuO in CuF binary systems favors the coherent rotation of the magnetic dipoles along the field direction, in contrast to the physically mixed two-phase nanoparticles with lack/weak of coupling.⁴⁷ The exchange interaction in CuF nanogranular systems is confirmed from the small shift in magnetic hysteresis curves recorded at range of fields from 0 to 40 kA/m under field cooled condition (not shown). It is also expected that CuFe₂O₄ and CuO of similar crystallite sizes favor better exchange and/or interparticle interaction when compared with the phases of dissimilar crystallite sizes, which will effectively affect the magnetic hyperthermia heating efficiency. An exchange bias effect was not experimentally observed at room temperature. However, it cannot be completely neglected in heat generation.³⁴ We believe that for interacting particles, the effective energy barrier depends

on both its anisotropy energy and the average of dipolar or exchange interactions.⁴⁰

3.3 | Magnetic hyperthermia of ferrites

The magnetic hyperthermia measurements were performed using the same mass (25 mg) of dry powder samples at room temperature. The temperature change ($\Delta T = T_i - T_0$, where T_0 and T_i are the initial and the temperature at i interval, respectively) was recorded as a function of time under different alternating (ac) magnetic fields and frequencies, whereas the heating rate ($\Delta T/\Delta t$) was estimated from the linear fitting of heating curve initial slopes. The measurement ON and OFF intervals have been decided based on the temperature change (ΔT), by keeping in mind that it should be kept below our temperature probe calibration ($\leq 80^\circ\text{C}$).

In the case of CFO NPs, the maximum ΔT reached where 35.1 and 33.5°C for CFO_UR and CFO_U0, respectively, under the highest applied field of 24 kA/m and 516 kHz within 300 s (Figure 5A,B). Lowering to 12 kA/m, the ΔT of both CFO NPs reached only about 40% of the maximum ΔT achieved at 24 kA/m (516 kHz), even increasing the frequency to 973 kHz (Figure 5C,D). The heating efficiency of both CFO NPs increases with the field amplitude at 516 kHz (Figure 5E). The frequency-dependent heating rate has also been elevated in the field of 12 kA/m (Figure 5F). Figure 5E shows that at higher field amplitude of 24 kA/m, the heating rate of CFO_UR seems to drop for the initial interval of time and later overshoot at longer interval time (Figure 5A), which might be due to two different heating rates (0.52 and 0.83°C/s for 10-20 s and 21 - 31 s, respectively) as it is reported earlier for cobalt ferrites.⁸ However, this is not observed in CFO_U0 NPs, as well as for the CuF binary systems discussed in the following section.

The heating curves of binary CuF nanogranular systems depict a much steeper ΔT increase within few seconds of measurement, where 61.5°C (at 30 seconds) and 48.9°C (at 130 seconds) are, respectively, achieved for CuF_20 and CuF_40 systems under 24 kA/m and a constant frequency of 516 kHz (Figure 6). For different frequencies but lower field (12 kA/m), the sample CuF_20 shows a maximum ΔT of 60.2°C after 60 seconds at 973 kHz, which is about 98% of the ΔT obtained at 516 kHz for 24 kA/m. The heating rates estimated for CuF systems are found to be linear with field at a constant frequency of 516 kHz (Figure 6E). However, at the higher frequency of 973 kHz, the heating rate of CuF_40 binary sample suddenly declined to 0.4°C/s (Figure 6D,F). The effect might not be due to two different heating rates, as it is observed in CFO_UR NPs, but to other factors. We assume that the exchange interaction between the different sizes of CuFe₂O₄ (20.8 nm) and CuO (28.9 nm) phases weakens and/or breaks down at higher frequency, where the magnetic

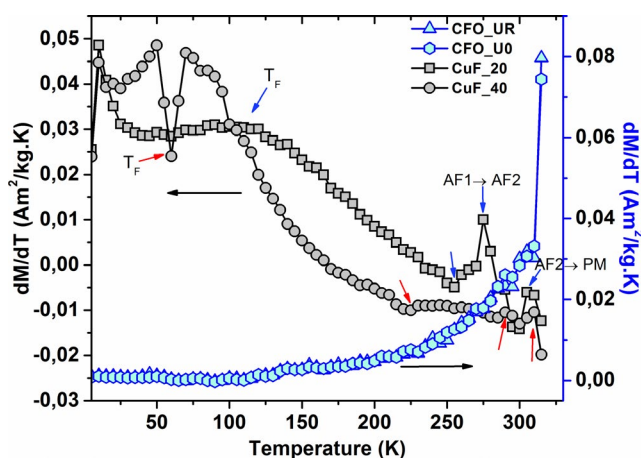


FIGURE 4 Derivatives of zero-field cooled magnetization as function of temperature (the blue and red arrows indicate the magnetic transitions)

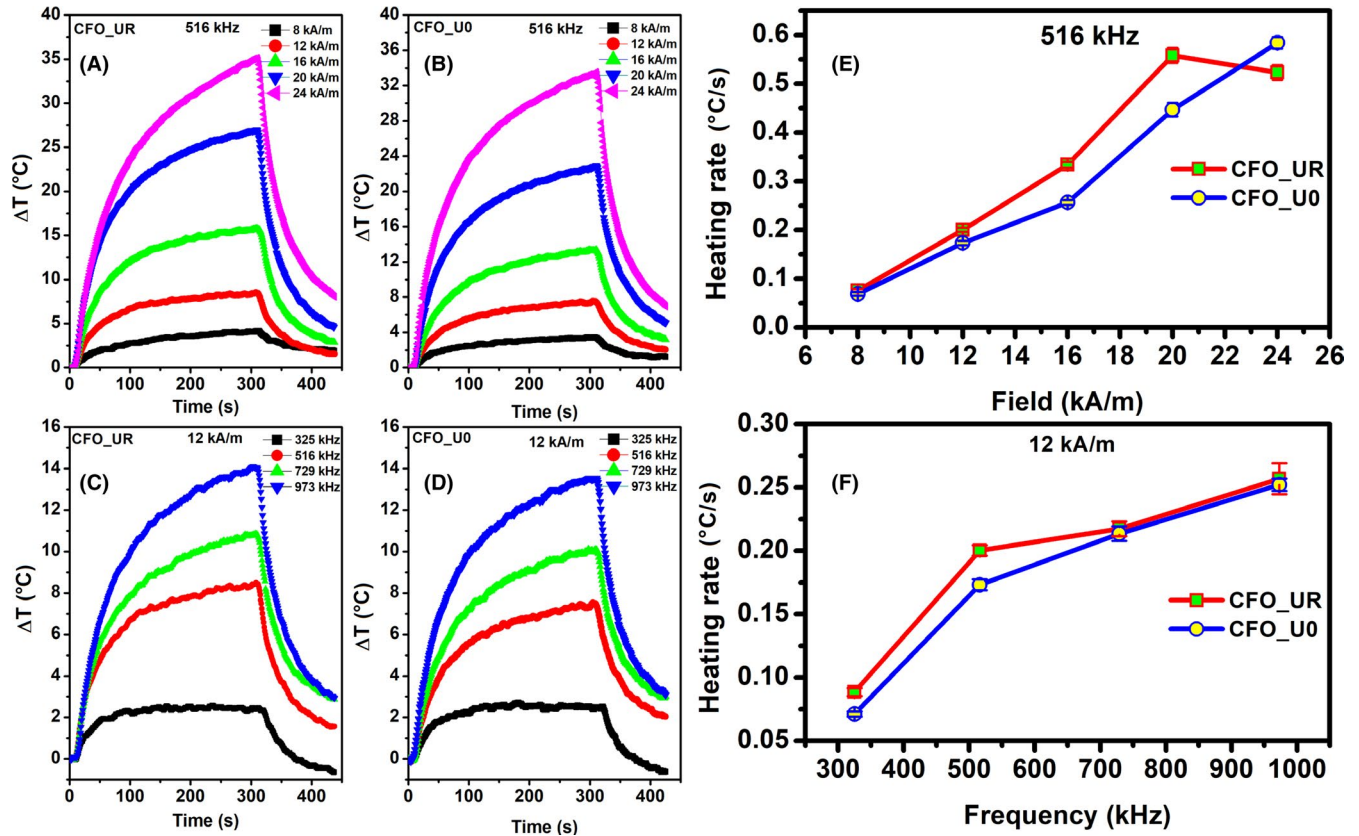


FIGURE 5 (A-D) Heating curve response to field and frequency and (E-F) the corresponding heating rate of CFO nanoparticles

domain rotation may not be achieved due to increased thermal energy. The heating rate depends on various factors such as particle size, saturation magnetization, anisotropy constant, exchange interaction, particle-particle interaction, etc.⁸ In addition, the heat loss in magnetic colloids mainly comes from the two mechanisms, Néel (τ_N) and Brownian relaxation (τ_B), whereas in the present system of ferrite nanopowders, it is mainly associated with τ_N as the measurements were done for dry powder samples.

We recollect from Table 2 that the saturation magnetization of chosen ferrites is almost equal, but with different coercivity and effective anisotropy constants. When comparing the heating rate of both CFO NPs, the sample CFO_UR, which is with a larger crystallite size and a smaller K_{eff} , found to be superior to CFO_U0, which exhibit a higher anisotropy constant. On the other side, CuF_20 shows better performance among CuF binary nanosystems. The aforementioned heating behavior of CFO has also been observed and reported for ferromagnetic Fe NPs of larger crystallite size with less anisotropy constant.⁴⁸ Indeed, the role of magnetic anisotropy on heating efficiency seems to be strongly dependent on the field amplitude. At low field, soft nanomagnets respond better, whereas at high field the opposite occurs (see figure 12 of Reference 8). In the experimental setup, due to the coercivity values for CFO, one

expects that the heating efficiency will increase for field amplitudes even higher than the one reported at 24 kA/m. Moreover, though the K_{eff} of CFO NPs is higher than that of CuF binary nanosystems, CFO does not show steeper increment under higher field amplitude as it is reported for cobalt ferrites.⁸ Although CFO nanoparticles have higher magnetization than CuF binary nanosystems, the dynamic hysteresis might be playing a role in the heat generation. It is well established that the magnetic response is strongly dependent not only on the magnetization but also on the magnetic anisotropy. Indeed, the dynamic hysteresis is strongly influenced by this term and shows optimum anisotropy values for hyperthermia.^{11,49} The τ_N of the ferrites varies in accordance with K_{eff} , and the volume of the ferrite particles (V), as given in,²¹

$$\tau_N = \tau_0 \exp \frac{K_{\text{eff}} V}{k_B T} \quad (2)$$

where τ_0 is the characteristic relaxation time approximately equal to 10^{-9} s, k_B and T are the Boltzmann constant and temperature, respectively (see Table 2). From the graphs (Figures 5 and 6), it is very clear that the heating rates of CFO_UR and CuF_20 show better efficiency compared to other ferrite samples. Binary CuF_20 nanosystem ($\text{CuFe}_2\text{O}_4/\text{CuO}$) with a

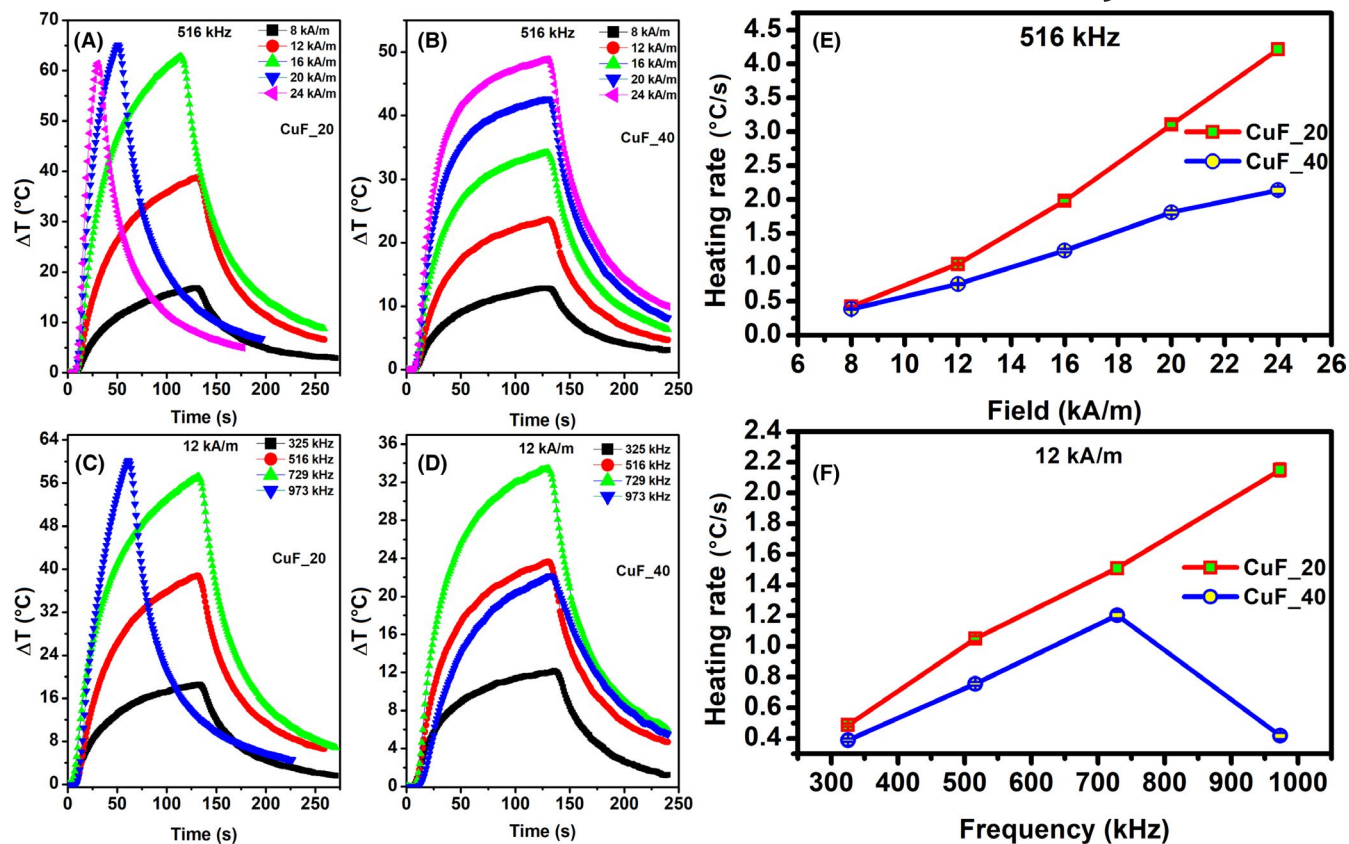


FIGURE 6 (A-D) Heating curve response to field and frequency and (E-F) the corresponding heating rate of CuF binary phase ferrite nanoparticles

similar crystallite size of about 28 nm is found to have larger magnitude than the others (4.2 and 2.15°C/s for, respectively, 516 kHz (24 kA/m) and 973 kHz (12 kA/m)). Hence, the particle size, broad particle size distribution, composition, intricate, and core/shell like structure might influence the heating efficiency of magnetic nanoparticles.²¹ Moreover, it is possible that since the coercivity of the cobalt ferrite NPs is higher, one expects that only a fraction of smaller particles will respond to the field, in such a way that the number of heat generators in the hard-like (CoFe₂O₄) particle is lower than the soft one (CuFe₂O₄/CuO).

To further discuss the effects of crystallite size, saturation magnetization, and K_{eff} on the enhancement of heating efficiency (assuming homogeneous nanoparticles), heating rate estimated at a low frequency (325 kHz), and magnetic field amplitude (12 kA/m) (though it is still above the biological limit, as they will inhibit harmful eddy currents in the human body⁵⁰) are considered (Figure 7). We observe that the heating rate of present ferrite nanoparticles increases with particle size, whereas it decreases for higher values of K_{eff} and τ_N (faster Néel relaxation showed worst heating efficiency). The heating rate of CFO NPs slightly follows the trend of magnetization, whereas it is not valid in the case of CuF binary

nanosystems. The higher effective magnetocrystalline anisotropy energy associated with the ferrite NPs restrains the magnetic rotation under given ac field amplitude and frequency.

Hence, we conclude that the crystallite size and effective anisotropy constant plays a key role in controlling the heating efficiency while the magnetization of the ferrites is similar. Moreover, nanogranular systems with two-phase CuFe₂O₄ and CuO compounds are found to be better thermoseeds than that of single-phase CFO NPs, where the exchange interaction and interparticle interaction might also have influenced the heating behavior. For the practical application, the biocompatibility of the thermoseeds is very important hence the suitable protective coating layer is necessary for the system of interest. The comparison of the present data with earlier reports become complicated as the heating efficiency depends on the approach to obtain the heating rate, mass fraction of ferrite nanoparticles, dispersion medium and measurement conditions such as frequency and field amplitude, whereas the particle size, K_{eff} , and magnetization are considered for the analysis.²¹ But we emphasize that the ferrites achieved through the present simple method yielded promising thermoseeds for the magnetic hyperthermia.

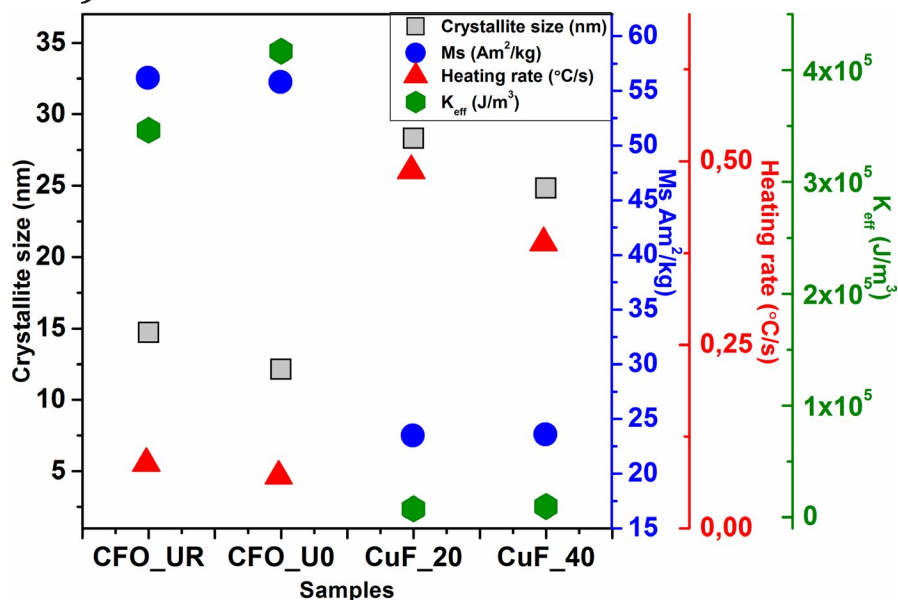


FIGURE 7 Relation between the crystallite size, magnetization, heating rate, and effective anisotropy constant of ferrite samples

4 | CONCLUSIONS

Thermosteeds, cobalt ferrite, and binary phase copper ferrite/copper oxide of two different sizes ((29 and 25 nm for $\text{CuFe}_2\text{O}_4/\text{CuO}$) and (15 and 12 nm for CoFe_2O_4)) were analyzed through structural and magnetic studies. The ferrite nanoparticles exhibited ferrimagnetic and superparamagnetic ordering for cobalt ferrite and copper ferrite binary nanogranular systems, respectively. The blocking temperature of ferrites varied with respect to particle size. The magnetic transition that corresponds to CuFe_2O_4 and CuO was evidenced. The heating efficiency as a function of magnetic field amplitude and frequency has been elaborated with respect to crystallite size, saturation magnetization, effective anisotropy constant, and Néel relaxation behavior. Indeed, the heating efficiency was highly influenced by crystallite size and effective anisotropy constant, whereas the magnetization was almost similar. Moreover, though the single-phase cobalt ferrite nanoparticles showed higher anisotropy energy, the binary phase copper ferrite nanogranular systems, with comparatively less anisotropy energy, exhibited superior heating efficiency of 4.21°C/s at field (24 kA/m) and frequency (516 kHz). It evidenced that, in addition to the particle size and effective anisotropy constant, the other factors such as exchange interaction and interparticle interaction might play a vital role in heating behavior. The particle size of the synthesized ferrites is within the permissible level (<30 nm) for the real-time application. And if they overcome by the agglomeration to achieve a highly stable biocompatible colloid then it would be a promising thermosteeds for magnetic hyperthermia application.


ACKNOWLEDGMENTS

The authors greatly acknowledge FONDECYT Postdoctoral Research Project No.: 3160170, CONICYT PIA/APOYOCCTE

AFB170007 and CONICYT BASAL CEDENNA FB0807, Government of Chile and FAPESP Postdoctoral Fellowship Process Number (2018) 19096-1, FAPESP thematic project number: 2017/10581-1, CNPq Grant number: 310230/2017-9, and FAPEG Grant number: 201710267000511, Government of Brazil for financial assistance.

ORCID

Prabhakaran Thandapani  <https://orcid.org/0000-0003-0245-8827>

Mangalaraja Ramalinga Viswanathan  <https://orcid.org/0000-0003-1016-9830>

Andris F. Bakuzis  <https://orcid.org/0000-0003-3366-106X>

Fanny Béron  <https://orcid.org/0000-0002-4926-2963>

Arun Thirumurugan  <https://orcid.org/0000-0001-7261-988X>

Juliano C. Denardin  <https://orcid.org/0000-0002-1373-6207>

Jose A. Jiménez  <https://orcid.org/0000-0003-4272-6873>

REFERENCES

1. Cancer. World heal organ. 2018. <https://www.who.int/news-room/fact-sheets/detail/cancer>
2. Nurgali K, Jagoe RT, Abalo R. Editorial: adverse effects of cancer chemotherapy: anything new to improve tolerance and reduce sequelae? *Front Pharmacol*. 2018;9:1–3. <https://doi.org/10.3389/fphar.2018.00245>.
3. Angelis CD. Side effects related to systemic cancer treatment: are we changing the promethean experience with molecularly targeted therapies? *Curr Oncol*. 2008;15(4):198–9.
4. Cubero DIG, Abdalla BMZ, Schoueri J, Lopes FI, Turke KC, Guzman J, et al. Cutaneous side effects of molecularly targeted therapies for the treatment of solid tumors. *Drugs Context*. 2018;7:212516. <https://doi.org/10.7573/dic.212516>
5. Datta NR, Ordóñez SG, Gaipil US, Paulides MM, Crezee H, Gellermann J, et al. Local hyperthermia combined with radiotherapy and/or chemotherapy: recent advances and promises

- for the future. *Cancer Treat Rev.* 2015;41(9):742–53. <https://doi.org/10.1016/J.CTRV.2015.05.009>
6. Amiri M, Niasari MS, Akbari A. Magnetic nanocarriers: evolution of spinel ferrites for medical applications. *Adv Colloid Interface Sci.* 2019;265:29–44. <https://doi.org/10.1016/j.cis.2019.01.003>
 7. deOuvinha OR, deMaria LCS, Barratt G. Nanomedicine and its applications to the treatment of prostate cancer. *Ann Pharm Fr.* 2014;72(5):303–16. <https://doi.org/10.1016/j.pharma.2014.04.006>
 8. Verde EL, Landi GT, Carrião MS, Drummond AL, Gomes JA, Vieira ED, et al. Field dependent transition to the non-linear regime in magnetic hyperthermia experiments: Comparison between maghemite, copper, zinc, nickel and cobalt ferrite nanoparticles of similar sizes. *AIP Adv.* 2012;2:032120. <https://doi.org/10.1063/1.4739533>
 9. Demirci CED, Manna PK, Nickel R, Aktürk S, Lierop JV. Comparative heating efficiency of cobalt-, manganese-, and nickel-ferrite nanoparticles for a hyperthermia agent in biomedicines. *ACS Appl Mater Interfaces.* 2019;11:6858–66. <https://doi.org/10.1021/acsami.8b22600>
 10. Wang G, Ma Y, Zhang L, Mu J, Zhang Z, Zhang X, et al. Facile synthesis of manganese ferrite/graphene oxide nanocomposites for controlled targeted drug delivery. *J Magn Magn Mater.* 2016;401:647–50. <https://doi.org/10.1016/j.jmmm.2015.10.096>
 11. Verde EL, Landi GT, Gomes JA, Sousa MH, Bakuzis AF. Magnetic hyperthermia investigation of cobalt ferrite nanoparticles: Comparison between experiment, linear response theory, and dynamic hysteresis simulations. *J Appl Phys.* 2012;111:123902. <https://doi.org/10.1063/1.4729271>
 12. Kim DH, Nikles DE, Johnson DT, Brazel CS. Heat generation of aqueously dispersed CoFe₂O₄ nanoparticles as heating agents for magnetically activated drug delivery and hyperthermia. *J Magn Magn Mater.* 2008;320(19):2390–6. <https://doi.org/10.1016/j.jmmm.2008.05.023>
 13. Silva MP, Drummond AL, Aquino VRR, Silva LP, Azevedo RB, Sales MJA, et al. Facile green synthesis of nanomagnets for modulating magnetohyperthermia: Tailoring size, shape and phase. *RSC Adv.* 2017;7(75):47669–80. <https://doi.org/10.1039/c7ra09446a>
 14. Mohammad F, Balaji G, Weber A, Uppu RM, Kumar CSSR. Influence of gold nanoshell on hyperthermia of superparamagnetic iron oxide nanoparticles. *J Phys Chem. C.* 2010;114:19194–201. <https://doi.org/10.1021/jp105807r>
 15. Mello FM, Rodrigues HF, Silveira-Lacerda E, Bakuzis AF, Zufelato N, Capistrano G. Precise determination of the heat delivery during in vivo magnetic nanoparticle hyperthermia with infrared thermography. *Phys Med Biol.* 2017;62(10):4062–82. <https://doi.org/10.1088/1361-6560/aa6793>
 16. Robles J, Das R, Glassell M, Phan MH, Srikanth H. Exchange-coupled Fe₃O₄/CoFe₂O₄ nanoparticles for advanced magnetic hyperthermia. *AIP Adv.* 2018;8:056719. <https://doi.org/10.1063/1.5007249>
 17. Nemati Z, Alonso J, Khurshid H, Phan MH, Srikanth H. Core/shell iron/iron oxide nanoparticles: are they promising for magnetic hyperthermia? *RSC Adv.* 2016;6:38697–702. <https://doi.org/10.1039/c6ra05064f>
 18. Lavorato G, Lima E, Vasquez Mansilla M, Troiani H, Zysler R, Winkler E. Bifunctional CoFe₂O₄/ZnO core/shell nanoparticles for magnetic fluid hyperthermia with controlled optical response. *J Phys Chem C.* 2018;122:3047–57. <https://doi.org/10.1021/acs.jpcc.7b11115>
 19. Hammad M, Hempelmann R. Enhanced specific absorption rate of bi-magnetic nanoparticles for heating applications. *Mater Chem Phys.* 2017;188:30–8. <https://doi.org/10.1016/J.MATCH.EMPHYS.2016.12.009>
 20. Lee JH, Jang JT, Choi JS, Moon SH, Noh SH, Kim JW, et al. Exchange-coupled magnetic nanoparticles for efficient heat induction. *Nat Nanotechnol.* 2011;6(7):418–22. <https://doi.org/10.1038/nnano.2011.95>
 21. Obaidat I, Issa B, Haik Y. Magnetic properties of magnetic nanoparticles for efficient hyperthermia. *Nanomaterials.* 2015;5:63–89. <https://doi.org/10.3390/nano5010063>
 22. Salas G, Veintemillas VS, Morales MDP. Relationship between physico-chemical properties of magnetic fluids and their heating capacity. *Int J Hyperthermia.* 2013;29(8):768–76. <https://doi.org/10.3109/02656736.2013.826824>
 23. Veverka M, Veverka P, Kaman O, Lančok A, Závěta K, Pollert E, et al. Magnetic heating by cobalt ferrite nanoparticles. *Nanotechnology.* 2007;18(34):345704. <https://doi.org/10.1088/0957-4484/18/34/345704>
 24. Yadavalli T, Jain H, Chandrasekharan G, Chennakesavulu R. Magnetic hyperthermia heating of cobalt ferrite nanoparticles prepared by low temperature ferrous sulfate based method. *AIP Adv.* 2016;5:055904. <https://doi.org/10.1063/1.4942951>
 25. Chatterjee BK, Bhattacharjee K, Dey A, Ghosh CK, Chattopadhyay KK. Influence of spherical assembly of copper ferrite nanoparticles on magnetic properties: Orientation of magnetic easy axis. *Dalton Trans.* 2014;43:7930–44. <https://doi.org/10.1039/c4dt00093e>
 26. Kumari P, Panda PK, Jha E, Pramanik N, Nisha K, Kumari K, et al. Molecular insight to in vitro biocompatibility of phytofabricated copper oxide nanoparticles with human embryonic kidney cells. *Nanomedicine.* 2018;13(19):2415–33. <https://doi.org/10.2217/nmm-2018-0175>
 27. Tran CD, Makuvaza J, Munson E, Bennett B. Biocompatible copper oxide nanoparticle composites from cellulose and chitosan: Facile synthesis, unique structure, and antimicrobial activity. *ACS Appl Mater Interfaces.* 2017;9:42503–15. <https://doi.org/10.1021/acsami.7b11969>
 28. Yan C, Tian Q, Yang S. Recent advances in the rational design of copper chalcogenide to enhance the photothermal conversion efficiency for the photothermal ablation of cancer cells. *RSC Adv.* 2017;7:37887–97. <https://doi.org/10.1039/c7ra05468h>
 29. Tian Q, Jiang F, Zou R, Liu Q, Chen Z, Zhu M, et al. Hydrophilic Cu₉S₅ nanocrystals: a photothermal agent with a 25.7% heat conversion efficiency for photothermal ablation of cancer cells in vivo. *ACS Nano.* 2011;5(12):9761–71. <https://doi.org/10.1021/nn203293t>
 30. Khanna L, Gupta G, Tripathi SK. Effect of size and silica coating on structural, magnetic as well as cytotoxicity properties of copper ferrite nanoparticles. *Mater Sci Eng C.* 2019;97:552–66. <https://doi.org/10.1016/j.msec.2018.12.051>
 31. Kanagesan S, Hashim M, AB Aziz S, Ismail I, Tamilselvan S, Alitheen N, et al. Evaluation of antioxidant and cytotoxicity activities of copper ferrite (CuFe₂O₄) and zinc ferrite (ZnFe₂O₄) nanoparticles synthesized by sol-gel self-combustion method. *Appl Sci.* 2016;6(9):1–13. <https://doi.org/10.3390/app6090184>
 32. Bohara RA, Thorat ND, Yadav HM, Pawar SH. One-step synthesis of uniform and biocompatible amine functionalized cobalt ferrite nanoparticles: a potential carrier for biomedical applications. *New J Chem.* 2014;38:2979–86. <https://doi.org/10.1039/c4nj00344f>

33. Shaw SK, Biswas A, Gangwar A, Maiti P, Prajapat CL, Meena SS, et al. Synthesis of exchange coupled nanoflowers for efficient magnetic hyperthermia. *J Magn Magn Mater*. 2019;484:437–44. <https://doi.org/10.1016/j.jmmm.2019.04.056>
34. Carrião MS, Bakuzis AF. Mean-field and linear regime approach to magnetic hyperthermia of core-shell nanoparticles: can tiny nanostructures fight cancer? *Nanoscale*. 2016;8(15):8363–77. <https://doi.org/10.1039/c5nr09093h>
35. Prabhakaran T, Mangalaraja RV, Denardin JC. Controlling the size and magnetic properties of nano CoFe_2O_4 by microwave assisted co-precipitation method. *Mater Res Express*. 2018;5:026102. <https://doi.org/10.1088/2053-1591/aaa73f>
36. Prabhakaran T, Mangalaraja RV, Denardin JC, Varaprasad K. The effect of capping agents on the structural and magnetic properties of cobalt ferrite nanoparticles. *J Mater Sci: Mater Electron*. 2018;29(14):11774–82. <https://doi.org/10.1007/s10854-018-9276-9>
37. Pearson's crystal structure database for inorganic compounds. 2015.
38. Gao YX, Zhu CM, Huang S, Tian ZM, Yuan SL. Size dependent training of exchange bias effect in $\text{CuFe}_2\text{O}_4/\text{CuO}$ nanocomposites. *J Magn Magn Mater*. 2017;439:384–90. <https://doi.org/10.1016/j.jmmm.2017.03.045>
39. Yin SY, Yuan SL, Tian ZM, Liu L, Wang CH, Zheng XF, et al. Effect of particle size on the exchange bias of Fe-doped CuO nanoparticles. *J Appl Phys*. 2010;107:043909. <https://doi.org/10.1063/1.3294618>
40. Goya GF, Rechenberg HR, Jiang JZ. Magnetic irreversibility and relaxation in CuFe_2O_4 nanoparticles. *J Magn Magn Mater*. 2000;218:221–8. [https://doi.org/10.1016/S0304-8853\(00\)00339-5](https://doi.org/10.1016/S0304-8853(00)00339-5)
41. Rao GN, Yao YD, Chen JW. Superparamagnetic behavior of antiferromagnetic CuO nanoparticles. *IEEE Trans. Magn*. 2005;41(10):3409–11. <https://doi.org/10.1109/TMAG.2005.855214>
42. He S, Zhang H, Liu Y, Sun F, Yu X, Li X, et al. Maximizing specific loss power for magnetic hyperthermia by hard–soft mixed ferrites. *Small*. 2018;14(29):1–9. <https://doi.org/10.1002/sml.20180135>
43. Kimura T, Sekio Y, Nakamura H, Siegrist T, Ramirez AP. Cupric oxide as an induced-multiferroic with high-TC. *Nat Mater*. 2008;7:291–4.
44. Wang F, Zou T, Liu Y, Yan L-Q, Sun Y. Persistent multiferroicity without magnetoelectric effects in CuO . *J Appl Phys*. 2011;110(5):54106. <https://doi.org/10.1063/1.3636106>
45. Charnaya EV, Lee MK, Tien C, Pak VN, Formus DV, Pirozerskii AL, et al. Magnetic and dielectric studies of multiferroic CuO nanoparticles confined to porous glass. *J Magn Magn Mater*. 2012;324(18):2921–5. <https://doi.org/10.1016/j.jmmm.2012.04.046>
46. Giovannetti G, Kumar S, Stroppa A, Brink VDJ, Picozzi S, Lorenzana J. High-Tc ferroelectricity emerging from magnetic degeneracy in cupric oxide. *Phys Rev Lett*. 2011;106:026401. <https://doi.org/10.1103/PhysRevLett.106.026401>
47. Nandwana V, Zhou R, Mohapatra J, Kim S, Prasad PV, Liu JP, et al. Exchange coupling in soft magnetic nanostructures and its direct effect on their theranostic properties. *ACS Appl Mater Interfaces*. 2018;10:27233–43. <https://doi.org/10.1021/acsami.8b09346>
48. Carrey J, Mehdaoui B, Respaud M. Simple models for dynamic hysteresis loop calculations of magnetic single-domain nanoparticles: application to magnetic hyperthermia optimization. *J Appl Phys*. 2011;109:083921. <https://doi.org/10.1063/1.3551582>
49. Aquino VRR, Vinícius-Araújo M, Shrivastava N, Sousa MH, Coaquira JAH, Bakuzis AF. Role of the fraction of blocked nanoparticles on the hyperthermia efficiency of Mn-based ferrites at clinically relevant conditions. *J Phys Chem C*. 2019;123:27725–34. <https://doi.org/10.1021/acs.jpcc.9b06599>
50. Rodrigues HF, Mello FM, Branquinho LC, Zufelato N, Silveira-Lacerda EP, Bakuzis AF. Real-time infrared thermography detection of magnetic nanoparticle hyperthermia in a murine model under a non-uniform field configuration. *Int J Hyperthermia*. 2013;29(8):752–67. <https://doi.org/10.3109/02656736.2013.839056>

How to cite this article: Thandapani P, Ramalinga Viswanathan M, Vinícius-Araújo M, et al. Single-phase and binary phase nanogranular ferrites for magnetic hyperthermia application. *J Am Ceram Soc*. 2020;00:1–12. <https://doi.org/10.1111/jace.17175>